Journal of Power Sources 195 (2010) 7701–7708

Contents lists available at ScienceDirect

Journal of Power Sources

journal homepage: www.elsevier.com/locate/jpowsour

Sulfonated poly (fluorenyl ether ketone) membrane with embedded silica rich layer and enhanced proton selectivity for vanadium redox flow battery

Dongyang Chen, Shuanjin Wang*, Min Xiao, Dongmei Han, Yuezhong Meng*

State Key Laboratory of Optoelectronic Materials and Technologie, The Key Laboratory of Low-carbon Chemistry & Energy Conservation of Guangdong Province, Sun Yat-Sen University, Guangzhou 510275, PR China

ARTICLE INFO

Article history:
Received 8 May 2010
Accepted 11 May 2010
Available online 19 May 2010

Keywords:
Vanadium redox flow battery
Proton exchange membrane
Composite materials

ABSTRACT

A series of novel organic–inorganic hybrid membranes with special microstructure, based on sulfonated poly (fluorenyl ether ketone) ionomer (SFPEK, IEC = 1.92 mequiv. g^{-1}) and SiO_2 or sulfonic acid group containing SiO_2 (SiO_2–SO_3H), has been successfully designed and prepared for vanadium redox flow battery (VRB) application. The SiO_2–SO_3H is synthesized by co-condensation of tetraethoxysilane and γ-propyl mercaptotrimethoxysilane via sol–gel process to control the same IEC with neat SPFEK. The hybrid membranes are prepared by simply adding the inorganic particles into the SPFEK solution in *N*,*N*′-dimethylacetamide, followed by ultrasonic dispersion, casting and profiled temperature drying process. The morphology is examined by SEM-EDX which is applied to the top surface, bottom surface and cross-section of the hybrid membranes. The water uptake, oxidative stability, thermal property, mechanical property, proton conductivity, VO^{2+} permeability and single cell performance are investigated in detail in order to understand the relationship between morphology and property of the membranes. All the hybrid membranes show dramatically improved proton selectivity at 20 °C and 40 °C when compared with Nafion117. The VRB assembled with the SPFEK/3%SiO_2 and SPFEK/9%SiO_2 membranes exhibit higher coulombic efficiency and average discharge voltage than the VRB assembled with the SPFEK membrane at all the tested current densities.

1. Introduction

Vanadium redox flow battery (VRB) has arisen as an advanced redox flow battery and attracted serious attentions over the last decade [1–4]. Besides holding the common merits such as lack of concentration polarization, it has overcome the inter-contamination of electrolytes by involving all vanadium ions as the redox couple. However, the permeation of electrolytes still causes capacity loss and consumes additional energy to recharge the battery. Furthermore, the permeabilities of different vanadium ions in a same membrane vary a lot owning to their different ionic sizes and electrostatic characters, which leads to asymmetric ion concentration in the electrolytes and affects the reproducibility of power generation. Therefore, the transport selectivity of membranes only for the charge carrying ions (in most cases, proton) is vital important for VRB application.

Nafion (DuPont) is the current benchmark material for proton exchange membrane because of its high proton conductivity and excellent chemical stability. Numerous works are focused on its morphology to develop appropriate models of proton conduction [5]. However, the permselectivity of Nafion should be enhanced especially for full hydrated state applications [3,6,7]. Mauritz et al. [8,9] initiated the *in situ* acid-catalyzed sol–gel technology to form a lot of Nafion/SiO_2 and Nafion/ORMOSIL composite membranes with the attempt to alter the transport properties of Nafion. Jiang et al. [10] reported the layer-by-layer self-assembly composite Nafion membrane with superior methanol blocking property. Vittadello et al. [11] prepared Nafion/hafnium oxide hybrid membranes by solution casting procedure and elucidated the effect of the amount of HfO_2 on the structure and performance of the membranes. Consequently, the application of Nafion was extended either by transforming the continuous hydrophilic pathway or surface shielding.

Aromatic condensation polymers are also extensively studied with the aim to substitute Nafion as low cost and high performance proton exchange membranes [12–14]. Because of the less pronounced hydrophilic/hydrophobic phase separation compared to Nafion, the proton transport channels in these membranes are narrower and more distorted while the proton conductivity can be tailored by the ion exchange capacity (IEC) [15]. Nevertheless, the narrower channels are beneficial for the proton selectivity owning to the filtration of large diameter ions. Further improvements on the performance of this kind of materials are achieved by lot

* Corresponding authors. Tel.: +86 20 84114113; fax: +86 20 84114113.
E-mail addresses: wangshj@mail.sysu.edu.cn (S. Wang), mengyzh@mail.sysu.edu.cn (Y. Meng).

0378-7753/$ – see front matter © 2010 Elsevier B.V. All rights reserved.
doi:10.1016/j.jpowsour.2010.05.026

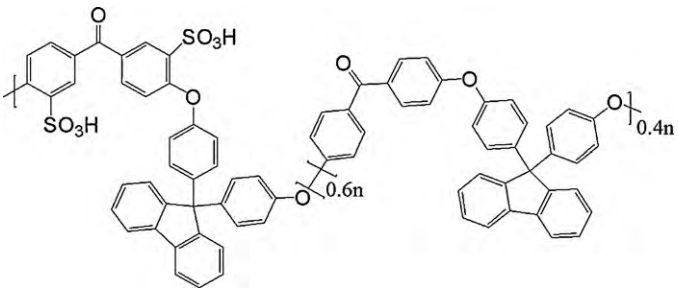

Fig. 1. Chemical structure of SPFEK.

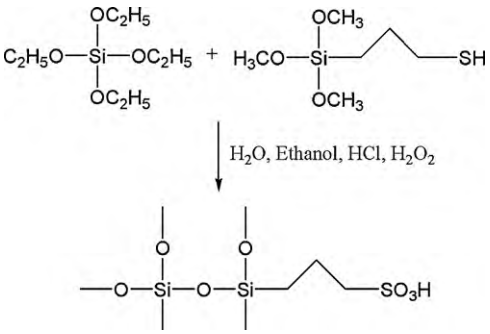

Scheme 1. Synthesis of SiO_2–SO_3H.

of methods such as hybridization [16,17], acid–base blend [18], surface coating [19], and cross-linking [20]. Demco et al. [21] investigated sulfonated poly (ether ether ketone)-silica membrane by ^1H solid-state NMR and concluded that the addition of small amount of silica can improve the proton conductivity of the membrane.

Previously, we have developed sulfonated poly (fluorenyl ether ketone) membrane (SFPEK, IEC = 1.92 mequiv. g^{-1}, depicted in Fig. 1) for the VRB application [22], which has shown lower electrolyte permeability and higher energy efficiency than Nafion117 in the single cell tests. In order to further reduce the electrolyte permeability while maintain a high proton conductivity level, herein, we report novel hybrid membranes based on SPFEK and SiO_2 or sulfonic acid group containing SiO_2 (SiO_2–SO_3H, IEC = 1.92 mequiv. g^{-1}) particles with silica rich layer embedded structure. We have previously prepared SPFEK/SiO_2 bulk hybrid membranes for the high temperature H_2/O_2 fuel cell application [23]. The addition of SiO_2 is to increase the water retention of the membranes at high temperatures (>100 °C). As to reduce the electrolyte permeation, the membranes with the embeded microstructure are expected to be more superior to the bulk hybrid membranes for the relative low resistance and the multilayer membranes for the absence of interface exfoliation. The physicochemical properties and electrochemical properties of these hybrid membranes were investigated in detail with the final cell performances and the morphology–property relationship of the membranes were discussed.

2. Experimental

2.1. Materials

Tetraethoxysilane (TEOS) and γ-propyl mercaptotrimethoxysilane (MPTMS) were obtained from Aldrich. SiO_2 powder with the average diameter of 50 nm was bought from Evonik Degussa, Germany. Nafion117 was supplied by DuPont Chemical. $VOSO_4 \cdot xH_2O$ was purchased from Shanghai LuYuan Fine Cheimical Plant, China, and was characterized by thermogravimetric mass spectrometry and oxidation–reduction titration. *N*,*N*′-dimethylacetamide (DMAc), concentrate sulfuric acid (95–98 wt%), ethanol, hydrochloric acid, potassium hydroxide, Sodium chloride and hydrogen peroxide (30 wt%) were obtained from commercial sources. All the chemicals were used as received.

2.2. Preparation of SiO_2–SO_3H particles

As depicted in Scheme 1, SiO_2–SO_3H particles with IEC = 1.92 mequiv. g^{-1} were synthesized via sol–gel process from TEOS and MPTMS with the molar ratio of TEOS:MPTMS = 173:30. To a 100 mL round bottom flask equipped with a nitrogen inlet and a condenser (also served as nitrogen outlet), 7.2 g TEOS, 1.2 g MPTMS, 20 mL H_2O and 20 mL ethanol were charged. The mixture was magnetically stirred at 50 °C. After adding of 10 mL H_2O_2 dropwise under nitrogen atmosphere, the reaction was continued for 24 h. Then the mixture was transferred to oven and heated at 80 °C for 3 h, 100 °C for 3 h and 120 °C for 24 h to carry out gelation. The product was grinded and washed by deionized water for many times. SiO_2–SO_3H particles were obtained at the high yield of 99.8%.

2.3. Preparation of hybrid membranes

The SPFEK/*x* wt%SiO_2 (or SPFEK/*x* wt%SiO_2–SO_3H) hybrid membranes were prepared by solution casting from their mixtures in DMAc. The *x* was set to be 3, 9 and 15, respectively. The mixtures were ultrasonic dispersed for 1 h and then spread on a glass plate in a dust-free environment to dry at 40 °C for 24 h and then at 80 °C under vacuum for 24 h. The ultrasonic dispersion ensures a uniform bulk distribution of silica while the low temperature evaporation of solvent needs long time and allows effective sedimentation of silica to form silica rich layer, as illustrated in Fig. 2. Sodium-form membranes were transformed into proton-form membrane by soaking in 0.5 M H_2SO_4 aqueous solution at 80 °C for 24 h. Excess acid was removed by immersing the membrane in deionized water at 80 °C for 24 h. The water was replaced for three times. All the membranes were stored in deionized water until used.

2.4. Membrane characterization

Fourier transform infrared spectroscopy (*FT-IR*). FT-IR spectra were recorded on a PerkinElmer Spectrum 100 Fourier transform spectrometer to confirm the chemical structure of components in the hybrid membranes.

Scanning electron microscopy (*SEM*). The distributions of silica at the top side, bottom side and cross-section of hybrid membranes were examined using a scanning electronmicroscopy (JSM-5600LV system of JEOL) equipped with an energy dispersive X-ray detector (EDX). The accelerating voltage was 15 kV. The cross-sections were obtained by cryo-fracturing samples in liquid nitrogen.

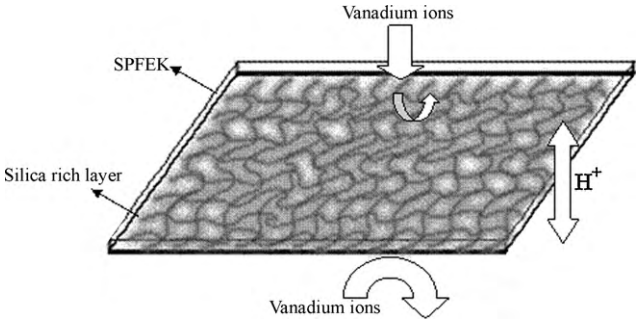

Fig. 2. Schematic illustration of configuration of silica rich layer embedded SPFEK.

Thermogravimetric analysis (*TGA*). Thermal stability was analyzed using a PerkinElmer Pyris Diamond TG/DTA analyzer. The temperature was increased from 50 °C to 150 °C and hold for 20 min to eliminate the absorbed water, and then elevated to 500 °C at a heating rate of 10 °C min^{-1} under N_2 atmosphere. The mass of samples was kept between 8 mg and 10 mg.

Water uptake. The dry membranes were weighed and immersed in deionized water at room temperature for 24 h. The water uptake was determined according to the following equation:

$$W(\%) = \frac{(W_w - W_d)}{W_d} \times 100\% \quad (1)$$

where W_d and W_w are the weight of membranes before and after water absorption, respectively.

Ion exchange capacity (*IEC*). IEC was measured by titration. The dried membrane was weighed and immersed in 1 M HCl solution for 5 h to give the membrane in *H*-form and then washed with excess amount of deionized water until PH was neutral. The membrane was then immersed in 2 M NaCl solution and the replaced proton was titrated using 0.1 M NaOH solution with phenolphthalein as indicator. IEC was calculated by following equation:

$$\mathrm{IEC} = \frac{\Delta V_{\mathrm{NaOH}} C_{\mathrm{NaOH}}}{W_d} \quad (2)$$

where W_d is the weight of the dry membrane, ΔV_{NaOH} is the comsumed volume of NaOH solution and C_{NaOH} is the concentration of NaOH solution.

Oxidative property. Oxidative stabilities were tested in Fenton's reagent (3 wt% H_2O_2 + 2 ppm $FeSO_4$) at 80 °C [24]. Membranes with the thickness ranging from 120 μm to 155 μm were dipped in Fenton's reagent conditioning at 80 °C water bath shaker. The values for each sample were determined from the times of commencement to break.

Mechanical properties. The tensile properties were determined by SANS (Shenzhen, China) electromechanical universal test machine (model CMT-4014). The tensile properties were determined at 20 ± 2 °C and 50% relative humidity. The samples were cut into dumbbell shape with the middle width of 2 mm. The crosshead speed was set at a constant of 2 mm min^{-1}. For each material been tested, three measurements were taken and the average value was recorded.

Proton conductivity. Membranes were kept at deionized water overnight prior to test. The proton conductivity (σ) was measured on a Solartron 1255 B frequency response analyzer coupled with a Solartron 1287 electrochemical interface. The impedance spectrum of a cell with the given membrane samples sandwiched between two gold electrodes was recorded. The conductivity was calculated from the impedance plot with a computer curve-fitting technique according to the electrode area of the cell and the thickness of the membrane, which was measured by a micrometer.

$$\sigma = \frac{d}{RS} \quad (3)$$

where *S* is the area of the electrode, *d* is the thickness of the membrane, and *R* is the impedance.

VO^{2+} permeability. The permeation of VO^{2+} was measured by the method similar to the literature [25]. 40 mL of 1 M $VOSO_4$ in 2 M H_2SO_4 solution and 40 mL of 1 M $MgSO_4$ in 2 M H_2SO_4 solution were filled respectively in two reservoirs which are separated by the membranes. $MgSO_4$ was used to equalize the osmotic pressure. The membrane area exposed to electrolytes was 5.3 cm^2. The two solutions were continuously magnetically stirred and the permeated concentration of VO^{2+} was measured by UV–vis spectrophotometer (Model: 752-P, Shanghai Xianke CO., China) at a time interval of 5 h at 20 ± 2 °C.

The VO^{2+} permeability was defined as VO^{2+} diffusion coefficients (*D*) of membranes determined by the Fick's first law of diffusion on the assumption of pseudo-steady-state condition inside the membrane, and is calculated by the following equation:

$$D = -\frac{J \times d}{|C_1 - C_2|} \quad (4)$$

where *J* is the flux of VO^{2+}, C_1 and C_2 are the concentrations of VO^{2+} in each side reservoir respectively, *d* is the thickness of the membrane.

2.5. Single cell testing

The single cell was fabricated using two graphite bipolar carved with serpentine flow field as electrodes and the hybrid membranes as separator. In order to minimize the resistance of the cell, the membranes were sandwiched in two pieces of carbon paper before being clamped by the electrodes. The anodic electrolyte was 2 M V^{2+} in 2 M H_2SO_4 solution and the cathodic electrolyte was 2 M VO_2^+ in 2 M H_2SO_4 solution, which were prepared by electro-oxidation and electro-reduction of 2 M $VOSO_4$ in 2 M H_2SO_4 solution, respectively. They were pumped through the cell unceasingly during the test at 20 ± 2 °C. The effective area of membrane was 4.86 cm^2 and the end voltage of discharging was set to be 0.75 V. The coulombic efficiency (CE) was calculated by the following equation:

$$\mathrm{CE} = \frac{C_d}{C_{tc}} \times 100\% \quad (5)$$

where C_d is the discharge capacity and C_{tc} is the theoretic charge capacity (where we assume the charge efficiency is 100%) of the cell.

3. Results and discussion

3.1. Compositional and morphological analysis

The representative FT-IR spectra for SiO_2, SiO_2–SO_3H, SPFEK, SPFEK/SiO_2 and SPFEK/SiO_2–SO_3H are shown in Fig. 3. In the spectra of SiO_2 and SiO_2–SO_3H, the peaks at 467 cm^{-1}, 796 cm^{-1}, 1120 cm^{-1}, 1638 cm^{-1} and 3436 cm^{-1} are observed, corresponding to Si–O–Si bending vibration, Si–O–Si asymmetric stretching vibration, Si–O–Si symmetric stretching vibration, H–O–H bending vibration of physisorbed water and –OH stretching vibration, respectively. There are additional peaks around 2924 cm^{-1} in the spectrum of SiO_2–SO_3H, which is ascribed to the C–H stretching vibration of methylene groups. Furthermore, the band centered at

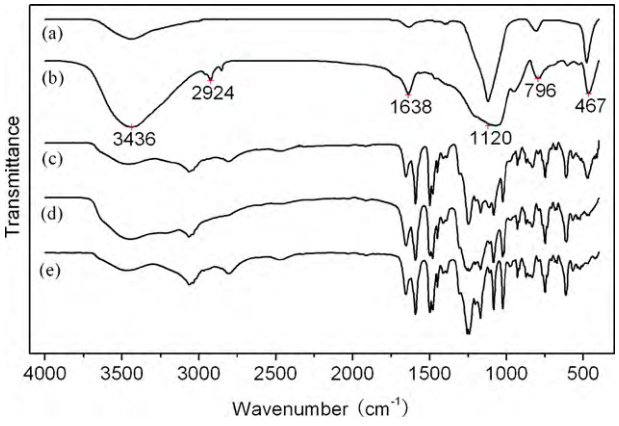

Fig. 3. FT-IR spectra of (a) SiO_2; (b) SiO_2–SO_3H; (c) SPFEK/15%SiO_2; (d) SPFEK/15%SiO_2–SO_3H; (e) SPFEK.

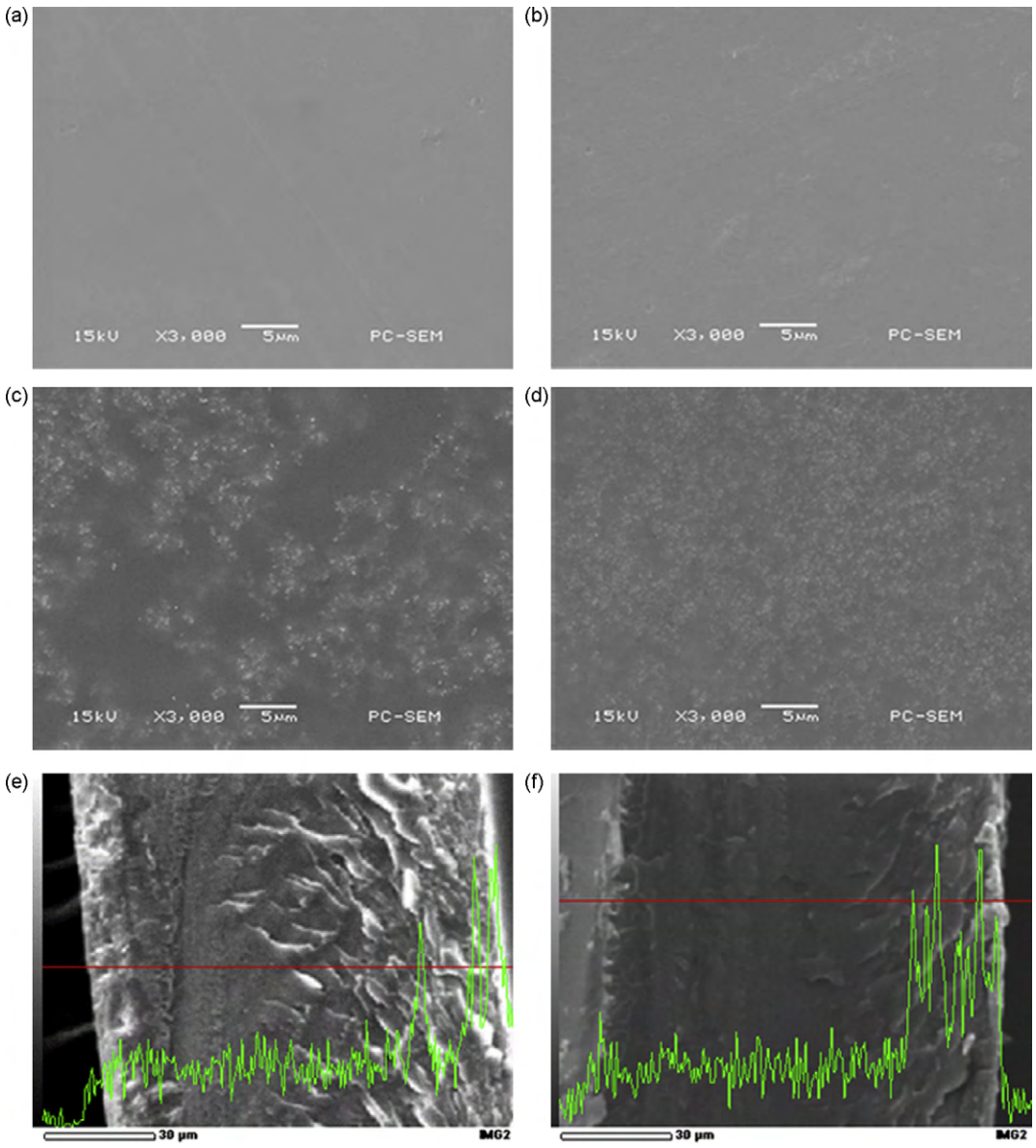

Fig. 4. Left column: SEM micrograph of SPFEK/15%SiO_2 (a) top side; (c) bottom side; (e) cross-section with silicon concentration profile along the membrane. Right column: SEM micrograph of SPFEK/15%SiO_2–SO_3H (b) top side; (d) bottom side; (f) cross-section with silicon concentration profile along the membrane.

1120 cm^{-1} is more complicated due to the overlap with S–O symmetric and asymmetric stretching vibration of sulfonic acid groups (1090 cm^{-1} and 1032 cm^{-1}). These provide evidence of the successful synthesis of polymeric ionomers with SiO_2–SO_3H groups. In the spectra of hybrid membranes, the band between 1000 cm^{-1} and 1400 cm^{-1} has become broader obviously compared to the spectrum of SPFEK, validating the existence of inorganic particles.

In order to probe the size and distribution of inorganic particles in the hybrid membranes, SEM-EDX was applied to the top surface, bottom surface and cross-section of the samples as depicted in Fig. 4. It can be seen that the top surfaces are smooth without any traces of inorganic particles while the bottom surfaces are uniform dispersed of inorganic particles. This result indicates the concentration difference of inorganic particles along the transverse direction of the hybrid membranes. This phenomenon has been reported in the literature [8]. In the literature, they merely reported the top surface with less inorganic particle content without further investigating the membrane properties of this microstructure. From the cross-section images with linear analysis of Si atom content along the direction by EDX, it can be seen that the inorganic particles are deposited at the bottom of the membranes forming 20–25% thickness layer. The layer is expected to be thinner with the lower content of the inorganic particles. All these observations are in good accordance with our proposed model shown in Fig. 2. From the images of bottom surface, we can see that the average size of inorganic particles is less than 100 nm, demonstrating no obvious aggregation of nano-particles occurred during membrane preparation. The SiO_2–SO_3H structure functions as a compatibilizer between SPFEK ionomer and SiO_2 because the smaller particle size with more uniform dispersion can be found in the corresponding SEM image. This is attributed to the propyl sulfonic acid groups modified the surface property of the inorganic particles.

3.2. Characterization of membrane properties

The water uptake plays an important role in the proton conduction (vehicle mechanism or Grotthuss mechanism). Generally, it increases with the increasing ion exchange capacity (IEC) of membranes as well as the working temperature. Although larger water uptake facilitates the proton transportation to a greater extent,

Table 1
Basic properties of the hybrid membranes compared with the pristine SPFEK.

Sample	IEC (mequiv. g^{-1})	Water uptake (%)	Oxidative time (min)	Tensile strength (MPa)	Elongation at break (%)	$T_{d-5\%}$ (°C)
SPFEK	1.92	39.0	85	27.7	49.4	330
SPFEK/3%SiO_2	1.83	36.6	93	29.1	23.5	332
SPFEK/9%SiO_2	1.57	29.8	138	31.2	14.4	343
SPFEK/15%SiO_2	1.26	25.0	144	33.8	13.4	355
SPFEK/3%SiO_2–SO_3H	1.92	44.1	73	32.7	43.8	354
SPFEK/9%SiO_2–SO_3H	1.92	46.2	70	35.4	35.1	358
SPFEK/15%SiO_2–SO_3H	1.92	47.0	68	36.9	32.6	361

excess amount of water may lead the membrane to dissolve. From Table 1, it can be seen that the SPFEK/SiO_2 hybrid membranes have lower water uptake compared to the SPFEK membrane at room temperature. This is because the membrane with doped SiO_2 has lower IEC value. For the SPFEK/SiO_2–SO_3H hybrid membranes, the IEC is designed to be the same as the neat SPFEK membrane (validated by titration). This can be simply achieved by adjudging the sulfonation degree of the polyionomers which used for hybrid preparation. However, the water uptakes increase with increasing the amount of SiO_2–SO_3H content after SiO_2 doped. This is due to the formation of ion clusters of SiO_2–SO_3H structure in the membrane. It has been reported that the water uptakes of membranes with larger ion clusters are higher than the membranes with smaller ion clusters at the same IEC value [26]. The ion clusters of SiO_2–SO_3H in the hybrid membranes are larger than the ion clusters of sulfonic acid groups in the SPFEK membrane. In this case, therefore, the water uptakes of the SPFEK/SiO_2–SO_3H hybrid membranes should be larger than the SPFEK membrane as proved in our experiments.

Fenton's reagent is often used to assess the stability of the membrane used in batteries. The highly reactive hydroxyl radicals generated by Fenton's reagent can destruct the molecular chain of SPFEK resulting in mechanical strength loss of the hybrid membranes. Herein, the oxidative stability was characterized by the time of membranes commencement to break (shown in Table 1) in Fenton's reagent. It should be noted that the SPFEK/SiO_2 hybrid membranes show significantly enhanced oxidative stability than the SPFEK membrane. This is owing to the lower water uptake of SPFEK/SiO_2 hybrid membranes which leads to fewer opportunities for the attack of hydroxyl radicals. Because the water uptakes of the SPFEK/SiO_2–SO_3H hybrid membranes are higher than the neat SPFEK membrane, the corresponding oxidative stabilities slightly decreased with further increasing SiO_2 content.

Fragile membranes always break into pieces after being clamped during battery cell assembling procedure, let alone tolerating the further impact of the electrolyte flows. Therefore, the mechanical integrity of membranes is especially important. As can be seen in Table 1, the tensile strength of the membranes increases from 27.7 MPa to 33.8 MPa with increasing SiO_2 content from 0% to 15%, while the elongation at break decreases from 49.4% to 13.4%. This is attributed to the inherent nature of inorganic/organic hybrid materials, i.e., the introduction of inorganic fillers can enhance the tensile strength but decrease the toughness of the inorganic/organic composites. Moreover, the doped SiO_2 can also expand the polymer matrix, weaken the interaction of relevant macromolecules and reduce the number of being pulled molecules at the certain thickness. Since the hydrophobic propyl chain of SiO_2–SO_3H is more compatible with SPFEK than SiO_2, the elongation at break only showed little decreases. All these hybrid membranes possess enough mechanical integrity for the vanadium redox flow battery (VRB) application.

The effects of SiO_2 and SiO_2–SO_3H dopants on the thermal characteristics of SPFEK were investigated by thermogravimetric analysis (TGA) method as shown in Fig. 5. It can be seen that the entire hybrid membranes exhibit improved thermal stability in comparison with neat SPFEK membrane. For the SPFEK/SiO_2 hybrid membranes, the TG profiles are almost the same with that of SPFEK membrane, with little shifting to higher temperature. This demonstrates that the relative thermal stable SiO_2 only increases the decomposition temperature without altering the decomposition mechanism of SPFEK. For the SPFEK/SiO_2–SO_3H hybrid membranes, the changes of TG curves are nearly independent of different SiO_2–SO_3H contents. An obvious different is observed compared with the TG curve of SPFEK membrane. The TG curves of SPFEK/SiO_2–SO_3H hybrid membranes lie in the middle of the TG curve of SiO_2–SO_3H powder and the SPFEK membrane. This implies the existence of chemical interaction between SiO_2–SO_3H and SPFEK, indicating a different decomposition mechanism is involved. The 5% weight loss temperatures for all the samples are listed in Table 1. Generally, the proton exchange membranes with higher ion exchange capacity (IEC) degrade more quickly than those with lower IEC [27–29]. However, it can be seen that the SPFEK/SiO_2–SO_3H hybrid membranes with the higher IEC values possess higher thermal stability than the SPFEK/SiO_2 hybrid membranes at the same inorganic dopant loading level. This further validates our above deduction of different decomposition mechanism involved in the thermogravimetric characterization.

The proton conductivity, VO^{2+} permeability and Φ (proton selectivity, defined as the ratio of proton conductivity to VO^{2+} permeability) of the hybrid membranes, pristine SPFEK and Nafion117 membrane measured at 20 °C and 40 °C under 100% relative humidity are listed in Table 2. The high proton conductivity of a membrane is responsible for the low resistance, high discharge voltage and large limiting current density of the cell that it is assembled. However, the conduction of cations in the electrolytes, which always accompany the conduction of protons, will reduce the cell capacity and lower the open circuit voltage as well as the discharge voltage. Therefore, the membrane with high proton selectivity is demanded for VRB application.

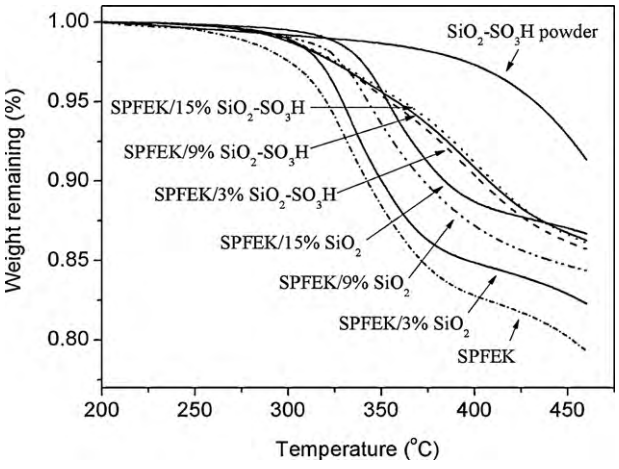

Fig. 5. Thermogravimetric analysis (TGA) of SPFEK, SiO_2–SO_3H powder and hybrid membranes.

Table 2
Proton conductivity, VO^{2+} permeability and Φ of the hybrid membranes, pristine SPFEK and Nafion117 membrane.

Sample	Proton conductivity (10^{-2} S cm^{-1})		VO^{2+} permeability ($\times 10^{-12}$ m^2 s^{-1})		Φ	
	20 °C	40 °C	20 °C	40 °C	20 °C	40 °C
Nafion117	3.22	4.73	4.90	12.32	0.66	0.38
SPFEK	2.19	3.54	1.05	2.91	2.09	1.22
SPFEK/3%SiO_2	3.18	4.47	1.40	3.60	2.27	1.24
SPFEK/9%SiO_2	2.09	3.29	0.87	2.35	2.40	1.40
SPFEK/15%SiO_2	1.38	1.98	0.47	1.33	2.94	1.49
SPFEK/3%SiO_2–SO_3H	2.24	3.61	0.98	2.65	2.29	1.36
SPFEK/9%SiO_2–SO_3H	2.37	3.76	1.03	2.74	2.30	1.37
SPFEK/15%SiO_2–SO_3H	2.48	3.82	1.05	2.79	2.36	1.37

From Table 2 it can be seen that both the proton conductivity and VO^{2+} permeability increase with the temperature. The SPFEK/3%SiO_2 hybrid membrane has higher proton conductivity and VO^{2+} permeability than pristine SPFEK membrane. This is because the incompatible SiO_2 particles expanded the network of SPFEK resulting in larger cavities for the transportation of hydrated ions. The larger content of SiO_2 will fill the cavities itself and block the hydrophilic pathways, which is validated by the declines of proton conductivity and VO^{2+} permeability of SPFEK/9%SiO_2 and SPFEK/15%SiO_2 hybrid membranes. For the SPFEK/SiO_2–SO_2H hybrid membranes, the proton conductivities increased while the VO^{2+} permeabilities decreased slightly. This is due to the good adhesion between SiO_2–SO_3H particles and SPFEK matrix, while, the *in situ* formed silica rich layer with higher sulfonic acid group concentration favors the transportation of protons but suppresses the permeation of VO^{2+}. In conclusion, all the hybrid membranes have comparable proton conductivity and dramatically lower VO^{2+} permeability than Nafion.

In most cases, the disclosed hybrid membranes have higher blocking property for separate components with lower proton conductivity [6,30]. A compromise has to be achieved in order to improve the cell performances, which is characterized by proton selectivity in this work. It can be seen in Table 2 that the hybrid membranes show enhanced proton selectivity than pristine SPFEK membrane. The proton selectivities of Nafion117 membrane at 20 °C and 40 °C were used for easier comparison, demonstrating its tremendous lower value when compared to the pristine SPFEK membrane and the hybrid membranes.

3.3. Single cell performance

The curves of the discharge voltages versus discharge times of the VRBs assembled with the hybrid membranes and the SPFEK membrane at the current densities of 20 mA cm^{-2} and 60 mA cm^{-2} are shown in Fig. 6. The voltage efficiency, which is represented by the discharge voltage, is mainly influenced by the resistance of the membrane. However, the coulombic efficiency of different cells, which is showed by the discharge time when the discharge current is the same, is affected by the resistance as well as the vanadium ions permeability of the membrane. It can be seen that for the VRB-SPFEK/SiO_2 and VRB-SPFEK, the changing tendency of discharge voltage is as follows: VRB-SPFEK/3%SiO_2 > VRB-

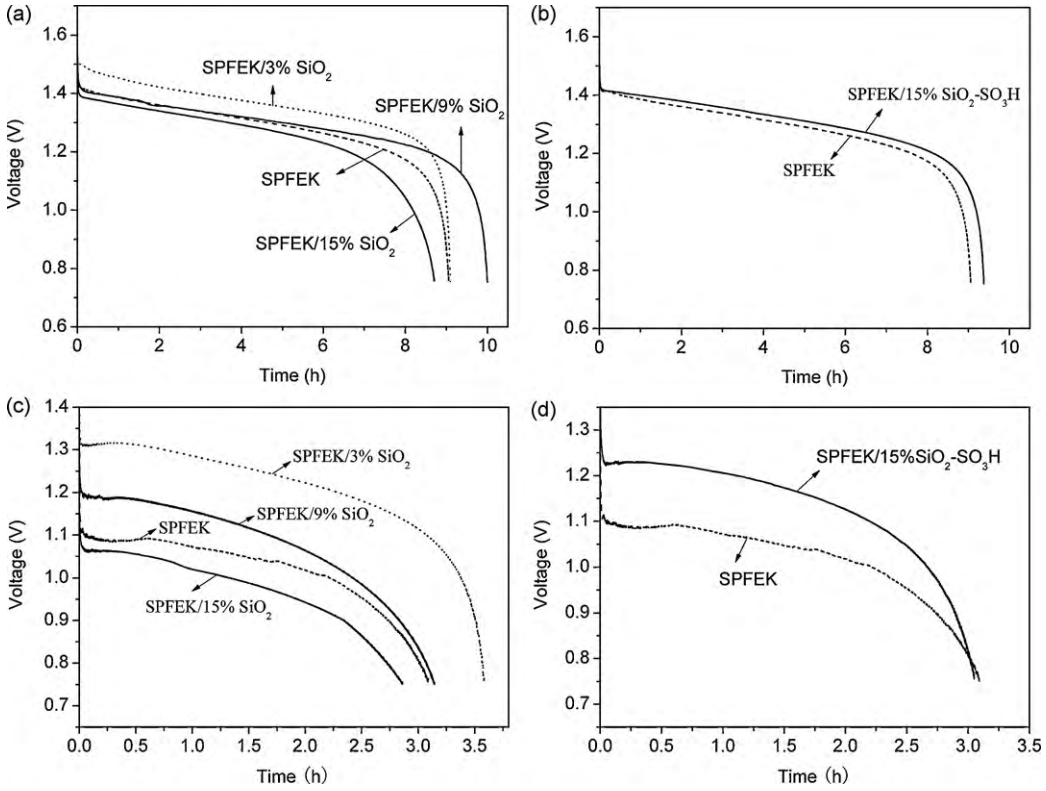

Fig. 6. Discharge characteristics of VRB assembled with (a) SPFEK/SiO_2 and (b) SPFEK/15%SiO_2–SO_3H hybrid membranes at 20 mA cm^{-2}; (c) SPFEK/SiO_2 and (d) SPFEK/15%SiO_2–SO_3H hybrid membranes at 60 mA cm^{-2}.

Table 3
The resistance and thickness of SPFEK and SFPEK/SiO_2 hybrid membranes at 20 °C.

Samples	SPFEK	SPFEK/3%SiO_2	SPFEK/9%SiO_2	SPFEK/15%SiO_2
Resistance (Ω)	0.93	0.62	0.87	1.46
Thickness (μm)	161	155	142	158

SPFEK/9%SiO_2 > VRB-SPFEK > VRB-SPFEK/15%SiO_2. This is in good accordance with the resistance of the membranes as shown in Table 3. The changing trend of coulombic efficiency at the current density of 60 mA cm^{-2} is the same as that of discharge voltage. Nevertheless, the changing trend of coulombic efficiency at the current density of 20 mA cm^{-2} is as follows: VRB-SPFEK/9%SiO_2 > VRB-SPFEK/3%SiO_2 > VRB-SPFEK > VRB-SPFEK/15%SiO_2. Because the coulombic efficiency is mainly influenced by the resistance at high current densities and by the electrolyte permeation at low current densities, the coulombic efficiency of VRB-SPFEK/3%SiO_2 is lower than that of VRB-SPFEK/9%SiO_2 at low current densities, since the VO^{2+} permeability of SPFEK/3%SiO_2 membrane is obviously larger than that of SPFEK/9%SiO_2 membrane. As demonstrated, the coulombic efficiencies of VRB assembled with other membranes are dominated by the membrane resistances. There is no obvious difference in the discharge characteristics of the VRBs assembled with different SPFEK/SiO_2–SO_3H hybrid membranes. A typical curve of VRB-SPFEK/15%SiO_2–SO_3H is shown as a representative. It can be seen that the voltage efficiency and coulombic efficiency of VRB-SPFEK/15%SiO_2–SO_3H are little higher than that of VRB-SPFEK at the current density of 20 mA cm^{-2}, and the discrepancy in voltage efficiency is more significant at the current density of 60 mA cm^{-2}.

The coulombic efficiencies of VRBs at different discharge current densities are shown in Fig. 7. The performance of VRB-Nafion117 is also depicted for comparison. It can be seen that all the coulombic efficiencies increase with the increasing of discharge current densities at the beginning and then decrease afterward. The higher discharge current density will lead to shorter discharge time (leading to fewer electrolytes permeation) and higher polarization (leading to lower energy conversion). The interaction of these two factors determines the characteristics of the coulombic efficiency at different current densities. The highest coulombic efficiencies of 90.8% at the current density of 20 mA cm^{-2} for VRB-SPFEK/9%SiO_2 and 96.7% at the current density of 60 mA cm^{-2} for VRB-SPFEK/3%SiO_2 are achieved respectively. Compared with VRB-SPFEK, the VRB-SPFEK/3%SiO_2 and VRB-SPFEK/9%SiO_2 show improved coulombic efficiency at all the tested current densities.

The effect of average discharge voltage on current density of the VRB assembled with SPFEK and hybrid membranes are shown in Fig. 8. It is apparent that the average discharge voltage

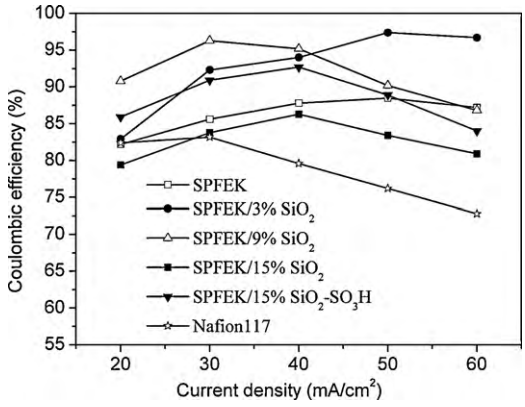

Fig. 7. Effect of current density on coulombic efficiency (CE) of the VRB assembled with Nafion117, SPFEK, and hybrid membranes.

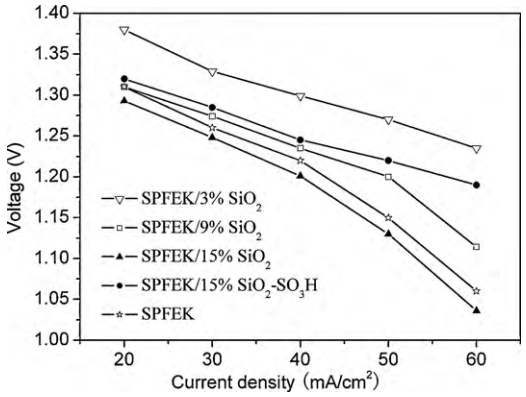

Fig. 8. Effect of current density on average discharge voltage of the VRB assembled with SPFEK and hybrid membranes.

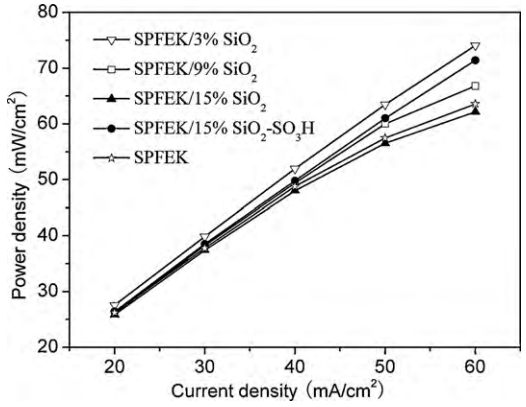

Fig. 9. Relationship of power density and current density of the VRB assembled with SPFEK and hybrid membranes.

decrease with the increasing of membrane resistance and discharge current density. The VRB-SPFEK/3%SiO_2, VRB-SPFEK/9%SiO_2 and VRB-SPFEK/SiO_2–SO_3H possess higher average discharge voltage than the VRB-SPFEK at all the tested current densities. From Fig. 9 it can be seen that the power densities increase sensitively with increasing discharge current densities. The VRB-SPFEK/3%SiO_2 shows the highest power density among all the VRB assembled.

4. Conclusions

Organic–inorganic hybrid membranes based on sulfonated poly (fluorenyl ether ketone) membrane (SFPEK, IEC = 1.92 mequiv. g^{-1}) and SiO_2 or SiO_2–SO_3H (IEC = 1.92 mequiv. g^{-1}) were prepared by solution casting procedure. The SiO_2–SO_3H can be readily synthesized by sol–gel reaction of tetraethoxysilane (TEOS) and γ-propyl mercaptotrimethoxysilane (MPTMS) with the aim to exclude the influence of IEC change on the properties of the hybrid membranes. The distribution of silica was found to be uniform arranged along with the parallel direction of the membrane and asymmetric along with the transverse direction of the membrane. The results demonstrated that a special membrane with silica rich layer in the bottom of the SPFEK membrane is formed.

The SPFEK/SiO_2 hybrid membranes exhibit higher thermal and oxidative stability than pristine SPFEK membrane, together with superior mechanical properties. However, the SPFEK/SiO_2–SO_3H hybrid membranes show lower oxidative stability than pristine SPFEK membrane. All the hybrid membranes possess enhanced proton selectivity at various temperatures. The as-made membranes show dramatically higher proton selectivity when compared with Nafion117. The single VRB cell was assembled using

above membranes for performance evaluation. The coulombic efficiencies of all single cells increase with increasing discharge current density firstly and then decrease thereafter. The VRB-SPFEK/3%SiO_2 and VRB-SPFEK/9%SiO_2 show higher coulombic efficiency and voltage efficiency than the VRB-SPFEK at all the tested current densities. The VRB-SPFEK/SiO_2–SO_3H show higher voltage efficiency than the VRB-SPFEK at all tested current densities with improved coulombic efficiency at certain current densities.

Acknowledgments

The authors would like to thank the China High-Tech Development 863 Program (Grant No.: 2007AA03Z217), and Guangdong Province Sci & Tech Bureau (Key Strategic Project Grant No.: 2006A10704004, 2006B12401006) for financial support of this work.

References

[1] X.L. Luo, Z.Z. Lu, J.Y. Xi, Z.H. Wu, W.T. Zhu, L.Q. Chen, X.P. Qiu, J. Phys. Chem. B 109 (2005) 20310–20314.
[2] J.Y. Xi, Z.H. Wu, X.G. Teng, Y.T. Zhao, L.Q. Chen, X.P. Qiu, J. Mater. Chem. 18 (2008) 1232–1238.
[3] J. Zeng, C.P. Jiang, Y.H. Wang, J.W. Chen, S.F. Zhu, B.J. Zhao, R.L. Wang, Electrochem. Commun. 10 (2008) 372–375.
[4] P. Zhao, H.M. Zhang, H.T. Zhou, J. Chen, S.J. Gao, B.L. Yi, J. Power Sources 162 (2006) 1416–1420.
[5] K.A. Mauritz, R.B. Moore, Chem. Rev. 104 (2004) 4535–4585.
[6] T. Li, Y. Yang, J. Power Sources 187 (2009) 332–340.
[7] S.W. Tay, X.H. Zhang, Z.L. Liu, L. Hong, S.H. Chan, J. Membr. Sci. 321 (2008) 139–145.
[8] Q. Deng, R.B. Moore, K.A. Mauritz, Chem. Mater. 7 (1995) 2259–2268.
[9] K.A. Mauritz, Mater. Sci. Eng. C 6 (1998) 121–133.
[10] S.P. Jiang, Z.C. Liu, Z.Q. Tian, Adv. Mater. 18 (2006) 1068–1072.
[11] M. Vittadello, E. Negro, S. Lavina, G. Pace, A. Safari, V. Noto, J. Phys. Chem. B 112 (2008) 16590–16600.
[12] A.L. Rusanov, D. Likhatchev, P.V. Kostoglodov, K. Mullen, M. Klapper, Adv. Polym. Sci. 179 (2005) 83–134.
[13] D.Y. Chen, S.J. Wang, M. Xiao, Y.Z. Meng, Energy Environ. Sci. 3 (2010) 622–628.
[14] K. Miyatake, T. Shimura, T. Mikami, M. Watanabe, Chem. Commun. (2009) 6403–6405.
[15] K.D. Kreuer, J. Membr. Sci. 185 (2001) 29–39.
[16] K. Miyatake, T. Tombe, Y. Chikashige, H. Uchida, M. Watanabe, Angew. Chem. Int. Ed. 46 (2007) 6646–6649.
[17] C.K. Jia, J.G. Liu, C.W. Yan, J. Power Sources 195 (2010) 4380–4383.
[18] Y.Z. Fu, A. Manthiram, M.D. Guiver, Electrochem. Commun. 9 (2007) 905–910.
[19] S.L. Zhong, X.J. Cui, T.Z. Fu, H. Na, J. Power Sources 180 (2008) 23–28.
[20] X.M. Wu, G.H. He, S. Gu, Z.W. Hu, P.J. Yao, J. Membr. Sci. 295 (2007) 80–87.
[21] M. Baias, D.E. Demco, I. Colicchio, B. Blumich, M. Moller, Chem. Phys. Lett. 456 (2008) 227–230.
[22] D.Y. Chen, S.J. Wang, M. Xiao, Y.Z. Meng, J. Power Sources 195 (2010) 2089–2095.
[23] Y.F. Zhang, S.J. Wang, M. Xiao, S.G. Bian, Y.Z. Meng, Int. J. Hydrogen Energy 34 (2010) 4379–4386.
[24] Y.L. Chen, Y.Z. Meng, X.H. Li, A.S. Hay, Macromolecules 38 (2005) 10007–10013.
[25] E. Wiedemann, A. Heintz, R.N. Lichtenthaler, J. Membr. Sci. 141 (1998) 215–221.
[26] S.H. Tian, Y.Z. Meng, A.S. Allan, Macromolecules 42 (2009) 1153–1160.
[27] L. Wang, Y.Z. Meng, S.J. Wang, X.H. Li, M. Xiao, J. Polym. Sci., Part A: Polym. Chem. 43 (2005) 6411–6418.
[28] X.H. Ma, C.J. Zhang, G.Y. Xiao, D.Y. Yan, G.M. Sun, J. Polym. Sci., Part A: Polym. Chem. 46 (2008) 1755–1769.
[29] D.S. Kim, G.P. Robertson, Y.S. Kim, M.D. Guiver, Macromolecules 42 (2009) 957–963.
[30] D.S. Kim, H.B. Park, J.W. Rhim, Y.M. Lee, Solid State Ionics 176 (2005) 117–126.